Bending Sensors Based on Thin Films of Semitransparent Bithiophene-Fulleropyrrolidine Bisadducts

Clara Chiappara,[†][a] Vincenzo Campisciano,[†][b] Giuseppe Arrabito,[c] Vito Errico,[d] Giovanni Saggio,[d] Gianpiero Buscarino,[c] Michelangelo Scopelliti,[c] Michelangelo Gruttadauria,[b] Francesco Giacalone,*[b] and Bruno Pignataro*[c]

[a]   Dr. C. Chiappara
        Department of Physics and Chemistry - Emilio Segrè, and INSTM-UdR
        University of Palermo, Building 17
        Viale delle Scienze, Palermo 90128, Italy.
        E-mail: bruno.pignataro@unipa.it
[b]   Dr. V. Campisciano, Prof. M. Gruttadauria, Prof. F. Giacalone
        Department of Biological, Chemical and Pharmaceutical Sciences and Technologies
        University of Palermo, Building 17
        Viale delle Scienze, Palermo 90128, Italy.
        E-mail: francesco.giacalone@unipa.it
[c]   Dr. G. Arrabito, Dr. G. Buscarino, Dr. M. Scopelliti, Prof. B. Pignataro
        Department of Physics and Chemistry -Emilio Segrè,
        University of Palermo, Building 17
        Viale delle Scienze, Palermo 90128, Italy
[d]   Dr. V. Errico, Prof. G. Saggio
        Department of Electronic Engineering
        University of Roma "Tor Vergata"
        Via del Politecnico 1, 00133 Rome, Italy
† Dr. C. Chiappara and Dr. V. Campisciano equally contributed.

Abstract: In this study, a novel bithiophene-fulleropyrrolidine bisadducts system (bis-Th2PC$_{60}$) was synthesized and electropolymerized by chronoamperometry onto flexible ITO/PET substrates. The resulting semitransparent thin film was characterized by XPS, FT-IR, cyclic voltammetry and optical techniques, confirming the good outcome of the electropolymerization process. AFM investigations permitted to highlight an inherent disordered granular morphology, in which the grain-to-grain separation depends upon the application of bending. The electrical resistance of the thin film was characterized as function of bending (in the range 0°-90°), showing promising responsivity to low bending angles (10°-30°). The $\Delta R/R_0$ variations turn out to be 8%,16% and 20% for bending angles equal to 10°, 20° and 30°, respectively. This study represents a first step towards the understanding of piezoresistive properties in electropolymerized fullerenes-based thin films, opening up applications as bending sensor.

Introduction

Conjugated polymers are macromolecular systems featured with alternating double- and single-bonds that lead to several interesting optical and electronic properties of interest for applications in solar cells,[1] transistors,[2] and sensors.[3] Among them, fullerene containing polymers derivatives have been widely used as materials in organic photovoltaics because of their high electron mobility.[4] In particular, mono-adducts consisting of C$_{60}$ fullerene cages covalently linked to thiophene chains have shown excellent electron transport properties in solar cells[4b, 4c] and have recently resulted in excellent morphology modulators, when introduced in small quantities as additives in P3HT/PCBM heterojunctions.[5] Notably, within the fullerene-based materials, it is possible to modulate the structural and energetic disorder by adding side chains to the fullerene moieties, resulting in multi-adducts (bis- or tris-adducts).[6] Differently to mono-adducts,[5, 7] the side chains in the fullerene multi-adducts hinders the tight packing of fullerene cages and/or triggers disorder in the energy levels due to the presence of more isomers, as shown by Steiner et al.[8] who also proved that the contribution from isomeric disorder dominates over the steric disorder.[8] In principle, such intrinsic disorder in the multi-adduct fullerene molecular packing could be leveraged for engineering new materials with responsivity to mechanical strain (such as bending or deformation). More specifically, a mechanical deformation can induce a rearrangement of the molecular packing and in turn of the conductive network, ultimately causing the variation of the electronic conduction properties.[9] This property is defined as piezoresistivity and is observed in materials (such as silicon)[10] in which a mechanical strain leads to a change in the electrical resistivity.[11] Differently from piezoelectricity in which a mechanical deformation induces the generation of an electronic potential,[12] piezoresistivity is based on the spacing or the slippage of the conductive domains caused by the application of mechanical strain within the material structure, finally resulting in an increase of electrical resistance.[13] This property is fundamental for emerging applications of wearable electronics,[14] including electronics skins,[15] human motion detection,[16] human-machine interface,[16a, 17] and other ones.[18] In particular, bending

sensors[19] represents one of the most technologically relevant. Highly desired features of bend sensors include a simple fabrication approach, flexibility, transparency, and high sensitivity to tiny deformations[20] for angles lower than 30°,[21] which is critical for many emerging medical applications,[3a, 14, 16b, 22] such as the evaluation of back or shoulder bending. However, the combination of these attributes in a single material is challenging; research efforts have focused on engineering materials such as PEDOT:PSS,[23] organic hydrogels,[24] graphene,[25] MWCNTs-graphene composites[26] that can in part combine these properties. Most of the sensors based on carbon nanotubes or graphene are opaque, showing limitations as various fields required transparent devices including those to be mounted directly on the human skin.[20] Only few studies have shown the development of materials enabling transparent piezoresistive sensors.[27] Some transparent strain sensor based on carbon nanotube and graphene are reported, although showing disadvantages in terms of sensitivity.[28] Moreover, sensors based on PEDOT:PSS,[23] showed low deformation response, particularly at low angles, in addition to opacity.

In the scenario of piezoresistive sensors, fullerene-based materials have received little attention, mainly due to the difficulty in obtaining films displaying morphology suitable for piezoresistive-based applications. One example provided by Shi et al.[13a] features fullerene as a lubricating additive to reduce the internal friction force during crack propagation in a deformation sensor based on graphene oxide and silver nanowires. However, the resulting sensor is not transparent and is produced as a composite of different materials, resulting in a complex fabrication procedure. Thus, it is highly desired to define an easier solution-based approach for the direct single-step fabrication of a transparent piezoresistive material. In this regard, the electropolymerization of aromatic monomers could be a suitable approach, given the easiness and the adaptability to deposit the polymer directly on the transparent electrode surface, starting from small quantities of monomer.[29]

In this work, we embraced all the requirements of a simple fabrication approach, flexibility, semitransparency, and high sensitivity to tiny deformations for angles lower than 30°. In this regard, we reported the synthesis of a novel bithiophene-fulleropyrrolidine bisadduct (bis-Th2PC$_{60}$) molecular system that is electropolymerized under mild conditions onto flexible substrates, resulting in a semitransparent material, showing remarkable piezoresistive properties enabling the development of low angle, high sensitivity bend sensors.

Results and Discussion

Characterization of bis-Th2PC$_{60}$

The synthesis of bis-Th2PC$_{60}$ is reported in **Scheme 1** and involves a 1,3-dipolar cycloaddition between the azomethine ylide, formed by reaction of sarcosine and 2,2′-bithiophene-5-carboxaldehyde and fullerene (Prato reaction).[30]

Scheme 1. Synthesis of the new bis-Th2PC$_{60}$ monomer and its electropolymerization.
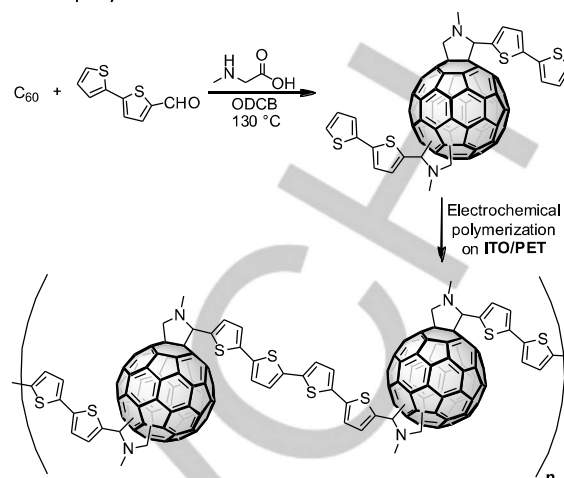
The ^{1}H NMR spectrum, FT-IR spectrum and UV-vis spectrum of the bis-Th2P-C$_{60}$ mixture, consisting of the purified less polar fraction of bisadducts (see Experimental), are shown in **Figure 1a-c**. The ^{1}H NMR spectrum resulted in a complicated pattern of partially overlapped signals due to the presence of different regioisomeric bisadducts.
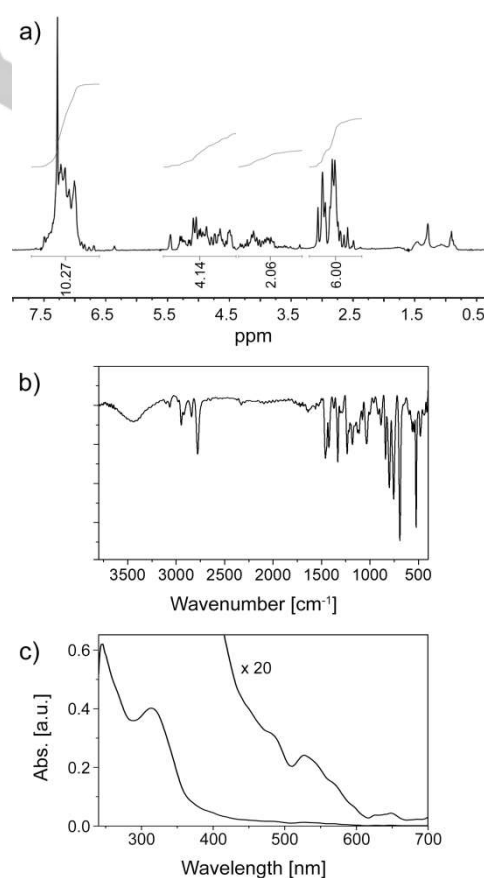

Figure 1. Characterization of the bis-Th2PC$_{60}$ monomer. (a) ^{1}H NMR (300 MHz, CDCl$_3$) spectrum (b) FT-IR (KBr) spectrum. (c) UV-vis spectra in chloroform (5.87E^{-6} M).

2

The functionalization of C_{60} with identical and symmetric addends could give eight possible isomers[31] but otherwise, as in the present case, this number increases because of the different relative orientation of the addends, thus justifying the complexity of the ^{1}H NMR spectrum. However, despite the great number of signals, it was possible to define three major regions in the NMR spectrum. In the first region between 7.12-6.79 ppm, there is resonance of the aromatic protons. In the 5.46-3.36 ppm region, resonate the fulleropyrrolidine ring protons, whereas signals centered at ca. 2.78 ppm are attributed to the methyl group protons.

In **Figure 1b**, the FT-IR spectrum shows the bands at 527, 1182, and 1424 cm^{-1} associated with the T_{1u} modes of the fullerene C_{60} cage. In addition, it is possible to identify bands in three main spectral regions: 850-650 cm^{-1} (C–S stretching), 1600-1400 cm^{-1} (C=C stretching) and 3200-2700 cm^{-1} (C–H stretching). As stated above, for our purposes, only the less polar fraction of bisadducts arising from a careful flash chromatography purification was used (see Experimental). In this regard, UV-vis spectrum of bis-Th2PC$_{60}$ (**Figure 1c**) allowed us to shed some light on the substitution patterns of the selected bisadducts mixture. Focusing attention on the 450-600 nm fingerprint region (magnification of **Figure 1c**), it is possible to note some similarity between the UV-vis spectrum of the bis-Th2PC$_{60}$ mixture and those of trans-2, trans-3, and trans-4 regioisomers of other fulleropyrrolidine bisadducts reported elsewhere.[31a, 32] Furthermore, this finding is in accordance with the elution order of such regioisomers, since among the different fulleropyrrolidine bisadducts trans regiosomers are the less polar and their polarity increases in the order trans-1<trans-2<trans-3<trans-4.

Although trans-1 constitutes the less polar of all trans regioisomers and therefore certainly it is included in the bis-Th2P-C$_{60}$ mixture, the observation of its peculiar UV-vis absorption is difficult because it is formed in smaller quantities than other isomers.[31a] The bands centered at 246 and 313 nm were attributed to the overlapped contribution of C_{60} core and bithiophene units (π → π* transition). In addition, before electropolymerization, it was necessary to investigate the electrochemical behavior of bis-Th2PC$_{60}$ monomer, to identify the electroactive species in the structure. The electrochemical behavior of the monomer was analyzed by means of CV measurements obtained on the GC electrode (**Figure 2**), while the measured anodic and cathodic peak potentials (E_{pa}, E_{pc}) are listed in Table 1.

Table 1. Electrochemical parameters (expressed in Volts) derived from the CV.[1]

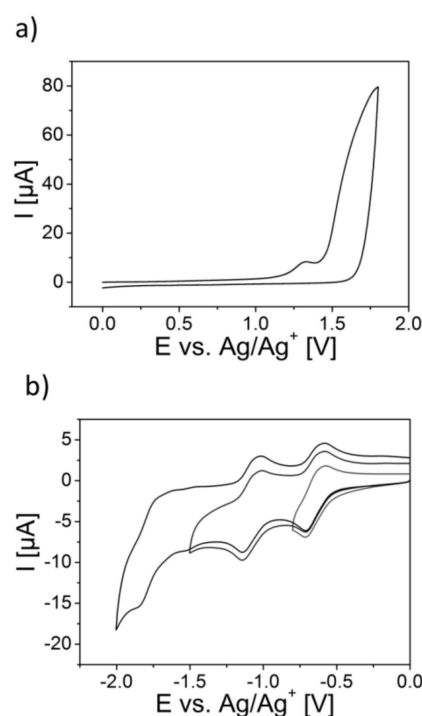| Compound	E^1_{pa}	E^1_{pc}	E^2_{pc}	E^3_{pc}	E^4_{pc}
bis-Th2PC$_{60}$	1.3	–0.72	–1.13	–1.80	–2.20
C$_{60}$	---	–0.53	–0.97	–1.50	–2.00

Figure 2. (a) Cyclic voltammogram in oxidation and (b) reduction of the bisTh2PC$_{60}$ acquired on GC in C$_6$H$_5$Cl-CH$_3$CN containing 0.1M TBAClO$_4$. Scan rate, 200 mV/s.

As shown in **Figure 2**, the bis-Th2PC$_{60}$ monomer displays an amphoteric redox behavior with an oxidation onset potential (E_{onset}) at 1.1 V and one oxidation peak potential at 1.3 V. These can be attributed to the oxidation of the bithiophene moieties,[33] and three reduction processes at -0.72 V, -1.13 V and -1.80 V versus Ag/Ag$^+$ which can be ascribed to the fullerene core. The cathodic peaks potentials are typical of the polythiophene fulleropyrrolidine systems,[29a] and they are shifted towards more negative potentials compared to those derived from the cyclic voltammogram of pure C_{60} (see **Figure S1a**). Also, the first and second reduction waves are reversible, while they become irreversible after scanning past the fourth reduction peak at -2.20 V (**Figure S1b**). This could be attributed to the fact that multiple reductions lead to chemical species of the monomer that in turn cause a high barrier to electron transfer and therefore more negative (positive) potentials are required to observe reduction reactions.[34]

Pbis-Th2PC$_{60}$ electrosynthesis and characterization

In order to achieve the oxidation of the monomer to form the corresponding polymer, the galvanostatic technique was used, i.e. polarizing the ITO/PET substrate at a constant potential of 1.5 V vs Ag/AgCl for 30 seconds to obtain a thin, semitransparent, homogeneous polymeric film on the electrode. A typical chronoamperometric deposition curve is shown in **Figure 3a**.

From the chronoamperometric curve, it is possible to estimate the thickness of the electrodeposited film by considering the equation[35]:

$$d = JMt/nF\rho$$

where d is the film thickness, J is the current density (mA/cm^2), M the molecular weight (g/mol), t the deposition time (sec), n the number of electrons, F the Faraday constant (96500 C) and ρ the density. A thickness of about 70 nm has been estimated, by approximating the molecular weight (1164 g/mol) to that of the monomer, the density (1.66 g/cm^3) of the C_{60} unit and imposing n=2.25.[33] This result is in agreement with other electrodeposition of polythiophenic systems.[33, 35] A more in-depth evaluation of the thickness was obtained by AFM scratching, as reported in **Figure S2**, following the approach explained by K. Biekowski and coworkers for electrodeposited films.[36] The evaluated thickness is about (26 ± 4 nm) in our experimental conditions. Such value is comparable for PEDOT electrodeposited films under similar deposition conditions.[37] Notably, the observed thickness is lower than the one estimated by calculating the whole charge deposited on the electrode. This can be likely explained since such calculation assumes the knowledge of the exact deposition mechanism, the density of the deposited material and, importantly, that all of the measured current (and hence charge) is due only to the deposited material as a result of the polymerization reaction.[29c]

Figure 3. (a) Chronoamperometric deposition at 1.5 V in an electrolytic solution containing C_6H_5Cl:CH_3CN, 0.1 M TBAClO$_4$ on ITO electrode. (b) XPS spectrum in the restricted C1s region. (c) Reflectance spectrum of the electropolymerized thin film on ITO/PET and (d) CV of the thin film electrodeposited on GC in a CH_3CN, 0.1M TBAClO$_4$ solution.

XPS and reflectance measurements were then carried out on the resulting Pbis-Th2PC$_{60}$ thin film in order to experimentally

determine the composition of the polymeric system. The XPS quantitative analysis of the electropolymerized Pbis-Th2PC$_{60}$ thin film resulted in the following elemental composition: C1s (80.7%), O1s (13.6%), N1s (1.7%) and S2p (2.4%). It is worth noticing that, In and Sn were not observed on film polymerized in mixture of C_6H_5Cl-CH_3CN in TBAClO$_4$, indicating a good surface coverage of the ITO substrate. Intriguingly, the polymer contains a single Cl species, (in Cl 2p spectra, 2p3/2-2p1/2 doublet at 207.0 and 209.0 eV respectively, **Figure S3a**), and two O species (O 1s spectra show two different species at 532.0 and 533.0 eV respectively, **Figure S3b**). The presence of chlorine and oxygen in these samples can be attributed to the ClO$_4^-$ counter-ion used during electrochemical copolymerization, which also causes the presence of oxygen.[38] The distribution of carbon species in the thin film is shown in **Figure 3b**. The distribution of carbon species was expressed as peak area percentages, resulting in the following values: C-C (75.32%), C-S (12.14%), C-N (7.32%), C=O (3.44%). The percentage distribution of the species confirms that the presence of carbon atoms deriving from fullerene cages are the predominant species in the material.

The reflectance spectrum of Pbis-Th2PC$_{60}$ (**Figure 3c**) shows two bands respectively at 230 and 310 nm of C_{60} and also a new band at 430 nm to be compared with the absorbance spectrum of the monomer in **Figure 1c**. This new band is attributed to the thiophenic conjugation in the polymer chain.[29a] Also, the UV-vis spectrum in **Figure S4** shows the semitransparency of the polymeric film with a transmittance of about 78% at 430 nm, corresponding to an absorbance value equal to 0.11. The region before 350 nm is not shown because of its noise due to the absorption of PET. For this reason, we acquired a reflectance spectrum, in order to explore the region of the spectrum between 200 to 350 nm, characteristic of the absorption of C_{60}. In addition, the FT-IR spectrum of Pbis-Th2PC$_{60}$ electropolymerized film confirms the presence of the functional groups which are characteristic of this polymeric system (see the **Figure S5**).

The electroactivity of Pbis-Th2PC$_{60}$ was investigated by CV on thin films electropolymerized by chronoamperometry on GC (see **Figure 3d**) in CH_3CN solution containing 0.1 M TBAClO$_4$. As can be seen from the oxidation process of the polymer in **Figure 3d**, the anodic peak disappears, while the E$_{onset}$ is shifted towards less positive potentials with respect to that of the monomer (**Figure 2a**). This result is attributed to the higher conjugation in the polymer chain in agreement with the reflectance spectrum above described. Instead, the reduction of the fullerene moieties in the polymer leads to changes of the cyclic voltammogram, compared to that of the monomer (**Figure 2b**). In particular, the first reduction wave of the polymer is shifted towards more negative potentials at -0.85 V and it is also irreversible. This could be attributed to the low electroactivity of the polymer likely due to structural disorder. Indeed, the reduction scan in the Pbis-Th2PC$_{60}$ cyclic voltammogram is typical of polymers obtained by the electropolymerization of bithiophene fulleropyrrolidines, further confirming the success of the synthetic approach.[39]
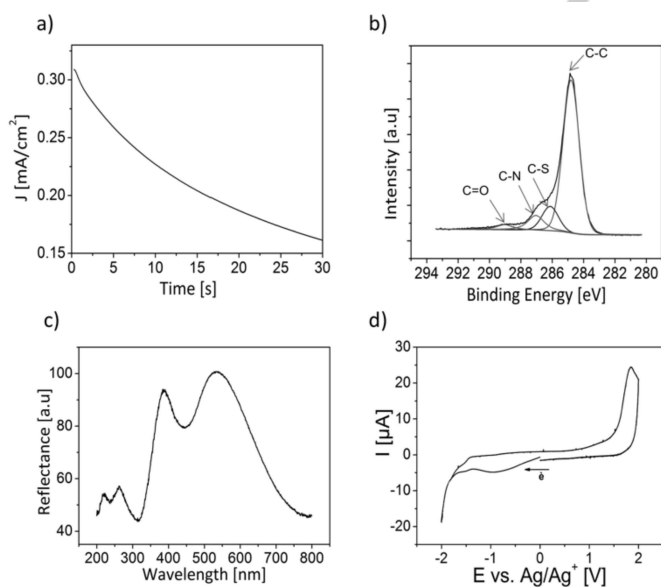
Characterization of the P(bis-Th2PC60) film morphology

The electrodeposited P(bis-Th2PC60) has a uniform distribution on the ITO electrode, as shown by the SEM characterization reported in **Figure S6**. The morphology of the deposited Pbis-Th2PC60 thin film was further investigated by AFM, as reported in **Figure 4**. Interestingly, the AFM characterization shows that Pbis-Th2PC60 thin film is constituted by a disordered network of globular grains (**Figure S7**), with lateral sizes in the 40-130 nm range (**Figure 4b)**, as measured on about 50 grains.
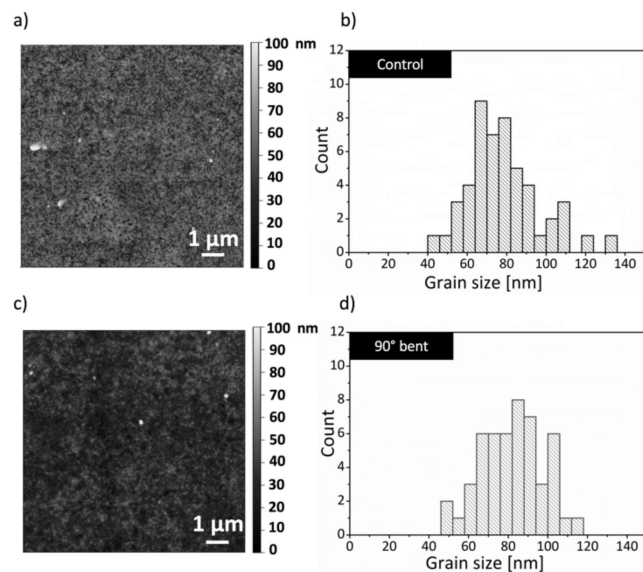

Figure 4. (a) AFM top image of the as deposited control film and (b) corresponding grain size distribution (N=50). (c) AFM top image of the film after bending and (d) corresponding grain size distribution (N=50).

The range of this grain sizes well agrees with the result of the Otsu's grain mark algorithm (see **Figure S8a**) on eight different 2 μm x 2 μm zones, which results in a mean grain size of 78 ± 8 nm. The average distance between the grains was determined by the threshold algorithm, that was implemented by setting 30 nm as height threshold, the zones this height having been considered as voids between the grains. As a result, the void sizes can be averaged to 35 ± 3 nm. To study the effect of deformation, the morphological investigation was extended to samples after a static bending of 90° (**Figure 4c**). In effect, bending causes a modification of the film morphology, since it leads to the formation of zones with a larger grain separation, as highlighted by the grain marking analysis images that were calculated following the same approach previously described (see **Figure S8b**), leading the formation of large voids that can be estimated in the 200-300 nm range. The grain sizes distribution on 1 μm x 1 μm (**Figure 4d**) and on the Otsu's grain mark value (77 ± 5 nm) are unmodified, whereas the grains distance is significantly increased, reaching 60 ± 7 nm, that is almost the double of the initial state (35 ± 3 nm). Moreover, it was not observed a significant difference by repeating the same bending (see **Figure S8c**), considering the grain size distribution (see **Figure S9**), the Otsu's grain mark (71 ± 6

nm) and the mean grains distance (equal to 57 ± 6 nm). The total number of grains was not significantly modified by bending, being in the range of 2500-2600 grains, estimated from a surface of 10 μm x 10 μm. Differently, bending induced an increase of the root mean square roughness (RMS) from 9.9 nm to about 12.0 nm. Such an increase in RMS is maintained by bending the substrate again at 90° (RMS = 12.7 nm).

These results can be explained by considering that bending triggers the formation of discontinuity and voids in the film. These defects add electrical discontinuity, potentially being a key factor for producing a significant electrical response under the film bending, in agreement with reported models on the piezoresistive sensing mechanism.[13] In fact, a simple expression based on the assumption of tunneling current, calculated by Zhang et al.[40] for modelling piezoresistivity in conductive polymer nanocomposites, permits to correlate the relative resistance R/R_0 change to the initial (s_0) and current (s) inter-particle average separation (γ is a constant):

$$\frac{R}{R_0} = \frac{s}{s_0}\exp[-\gamma(s_0 - s)]$$

Considering that the thickness (< 30 nm) is much lower than the width (5 mm) and length of the deposited film (7 mm), it is possible to estimate the initial sheet resistance of the uniform bidimensional film to be $R_s \approx 95k\Omega/sq$. The piezoresistivity properties of the Pbis-Th2PC60 thin film were verified by electrical measurements, which are below reported.

Piezoresistive characterization of the Pbis-Th2PC60 thin films

The fabrication of the sensor as reported in **Figure 5a** consists in electrically connecting the Pbis-Th2PC60 film produced on ITO/PET by using inkjet-printed silver electrodes. The resulting sensor (shown in **Figure 5b**) was placed on a motorized hinge (**Figure 5c**) for the electrical characterization. By looking at the inset in **Figure 5c,** the active area has to be fully interested in the bending action. The performance as a bend sensor was evaluated by measuring the electrical resistance upon bending in the angle range comprised between 0-90° forth and back. The typical $\Delta R/R_0$ variation as a function of the bending angle is reported in **Figure 5d**, whereas ΔR variation is reported in **Figure S10**. Moreover, the resistance variation for ten bending cycles is reported in **Figure 5e**, showing good bending angle detection repeatability. The sensor shows an interesting behavior at small bending angles, in the range comprised between 10°-30°, that could be suitable for applications demanding high precision for small bending angle. Remarkably, the $\Delta R/R_0$ variations at low bending angles (being around 8% for 10°, 16% for 20° and 20% for 30°) are comparable or even better than those reported bend sensors based on opaque materials typically ranging from 0.2% to 8% for 10°, from 0.3% to 12% for 20°, and from 0.6% to 18% for 30° bending.[23, 41] We associate the plateau at higher bending angles to the material behavior at the nanoscale. Indeed, differently from the currently reported piezoresistive materials that have conductive domains

and cracks in the micron-scale,[13a, 27a] the nanoscale separations among the nanosized grains of the Pbis-Th2PC$_{60}$, ultimately result in excellent sensitivity to tiny mechanical deformations and limited sensing range. This trend is well in agreement with the mechanisms of defects and grain separation that is triggered by mechanical deformation, following the piezoresistive sensing mechanism.[13a] Importantly, similar nanoscale separation between grains has been observed in PEDOT:PSS grains.[42] However, the $\Delta R/R_0$ variations of PEDOT-based bending sensors[23] are significantly lower in comparison to Pbis-Th2PC$_{60}$. This can be explained as follows. The PEDOT:PSS films are characterized by grains with a hydrophobic, highly conductive PEDOT rich core surrounded by a hydrophilic insulating PSS rich shells that interact with each other via hydrogen bonds based on HSO$_3$ groups between the PSS rich shells. As a remarkable difference, in the Pbis-Th2PC$_{60}$ film, the grain-to-grain interactions are significantly weaker, also resulting from the intrinsic disorder in the multi-adduct fullerene molecular packing. The lower cohesion between grains leads to a higher variation of $\Delta R/R_0$ at a low bending angle. We associate the plateau at higher bending angles to the material behavior at the nanoscale. Indeed, differently from the currently reported piezoresistive materials that have conductive domains and cracks in the micron-scale,[13a, 27a] the nanoscale separations among the nanosized grains of the Pbis-Th2PC$_{60}$, ultimately result in excellent sensitivity to tiny mechanical deformations and limited sensing range. In fact, the responsivity to larger bending angles is specifically connected to the slippage of the conductive domains, which likely cannot occur in the Pbis-Th2PC$_{60}$ thin film due to its nanosized grains. This trend is well in agreement with the mechanisms of defects and grain separation that is triggered by mechanical deformation, following the piezoresistive sensing mechanism.[13a]
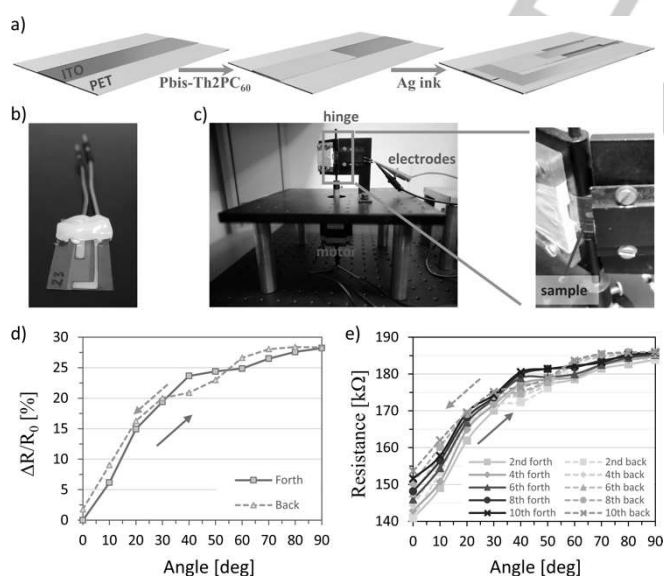

Figure 5. (a) Fabrication of the Pbis-Th2PC$_{60}$ based bend sensor. (b) Picture of the packaged sensor. (c) Picture of the motorized setup for the sample electrical characterization; the inset shows the sample positioning on the hinge. (d) Typical $\Delta R/R_0$ variation vs. bending angle. (e) sensor resistance when bending ten times from 0 to 90 degrees (forth) and 90 to 0 degrees (back); the graph shows only even measurements for graphical clarity.

Conclusions

This work shows the synthesis of a novel bithiophene-fulleropyrrolidine bisadducts system (Pbis-Th2PC$_{60}$) that can be electropolymerized under the form of thin film onto flexible ITO/PET substrates. This thin film evidences an inherent disordered morphology triggered by the presence of different regioisomeric bisadducts. The system results in a semitransparent piezoresistive bend sensor and likely due to the peculiar nanoscale separation between grains it is well responsive to deformations even at low bending angles. Importantly, this approach permits to obtain in a single step a piezoresistive material without the need to combine semiconductive/conductive materials within polymers matrices. The herein synthesized material is suitable for applications in bend sensors that require semitransparency, and sensitivity to small bending angles including those in the field of wearable electronics such as human motion, rehabilitation medicine, sport medicine and athletics, telemedicine, robotics and computer interfaces.

Experimental Section

Synthesis of bis-Th2PC$_{60}$

A solution of C$_{60}$ (500 mg, 0.69 mmol) in o-dichlorobenzene (o-DCB) (50 mL) was sonicated for 20 minutes before adding 2,2'-bithiophene-5-carboxaldehyde (336 mg, 1.73 mmol) and sarcosine (460 mg, 5.17 mmol). The resulting solution was stirred at 130 °C for 18 h. The mixture was allowed to reach room temperature and the solvent was removed under vacuum. The obtained dark residue was dissolved in chloroform, adsorbed onto silica by removing chloroform under vacuum and purified by silica gel chromatography. No unreacted fullerene C$_{60}$ was found and a gradient elution with a mixture of hexane/toluene (from 2:1 v/v to 1:1 v/v) was used to recover the monoadduct. Conversely, toluene/hexane 2:1 v/v was used to recover the less polar fraction of bisadducts, whereas another fraction was collected using toluene/hexane mixtures from 4:1 v/v to 8:1 v/v. These last two fractions, in accordance with the elution order of the regioisomers of other fulleropyrrolidine bisadducts reported elsewhere,[31a, 32] were mainly composed by the less polar *trans* regiosomers, and *cis* regioisomers as well as higher adducts,[43] respectively. For our purposes, only the isolated fraction containing the less polar bisadducts mixture was further purified by its dissolution in chloroform, precipitation with an excess of methanol and subsequent centrifugation. The supernatant was removed, the residue was dissolved in chloroform and precipitated with an excess of hexane. The precipitate was recovered and dried at 40°C under vacuum obtaining the bisadducts as a dark solid (180 mg; 22%). ^{1}H NMR (300 MHz, CDCl$_3$): see Figure 1a; FT-IR (KBr) v/cm^{-1} = 3104, 3066, 2947, 2919, 2840, 2778, 1460, 1424, 1331, 1234, 1181, 1034, 840, 800, 755, 691, 525, 480. UV-vis (CHCl$_3$): λ_{max}= 246, 313, 484, 527 nm.

Pbis-Th2PC$_{60}$ thin film preparation and characterization

Prior to each electrodeposition, the ITO/PET electrodes were patterned, removing the ITO with HCl 1M, then cleaned with methanol, acetone and propanol each for 10 minutes using an ultrasonic bath and finally cleaned by UV-ozone for 30 minutes. The electrodepositions were carried out by a three electrodes set-up. This includes the ITO/PET patterned working electrode (active area 5 mm x 12 mm), a reference Ag/AgCl electrode and a graphite counter electrode ensuring the current flow through the electrochemical cell. The three electrodes were immersed in an electrolytic solution comprising a $C_6H_5Cl:CH_3CN$ solvent mixture (2:1 v:v), the monomer at $4 \cdot 10^{-4}$ M concentration, and tetrabutylammonium perchlorate (TBAClO$_4$) 0.1 M as support electrolyte. All the electrochemical experiments were performed at room temperature under nitrogen flow at a pressure of 0.5 bar. The electrodeposition of bis-Th2PC$_{60}$ was performed by the galvanostatic method by a constant potential of 1.5 V. After the electrodeposition, the modified working electrode was washed with the solvent mixture employed in the synthesis to remove the supporting electrolyte and the unreacted monomer. The electrodeposited thin film was investigated by XPS using a ULVAC-PHI PHI 5000 Versa Probe II Scanning XPS Microprobe™, source Al Kα (1486.6 eV), 128 channels hemispherical analyzer, FAT mode. Also, reflectance spectra were recorded by using UV-vis spectrophotometry Jasco V-570. The electroactivity of the monomer and the electrodeposited thin film were investigated by cyclic voltammetry (CV) recorded with the Potentiostat/Galvanostat (Metrohm Autolab PGSTAT 128N) in a three-electrode cell using Glassy carbon (GC diameter = 3 mm, Bio-Logic SAS) as working electrode, platinum as counter electrode, and Ag/AgCl 3.5M KCl (Hanna Instruments) as reference electrode. Atomic Force Microscope (AFM) measurements were acquired in air by using a Bruker FAST-SCAN BIO microscope equipped with a closed-loop scanner (X, Y, Z maximum scan ranges: 35 mm, 35 mm, 3 mm, respectively). The scans were obtained in tapping mode, by using Bruker FASTSCAN-A© probes with an apical radius of about 5 nm. AFM images were obtained with a pixel resolution comparable to the tip size. The images were analyzed by the Gwyddion software (2.50 version). The grain sizes were evaluated on eight different 2 µm x 2 µm zones by the Otsu's grain marking algorithm. The voids between the grains were evaluated by the threshold algorithm (30 nm as height threshold). Thickness measurements were performed in air by a Bruker Dimension FastScan Bio microscope. At first, we scratched the film by a rigid AFM probe in a squared region with size 2 µm x 2 µm and then we measured the depth of the produced hole from the AFM image obtained in a region with size 10 µm x 10 µm centered in the position of the hole. Both the scratching process and the AFM image obtained by using a Bruker TESP probe (spring constant 40 N/m, tip radius 7-10 nm) in contact mode, but by using two orders of magnitude more force and faster scan rates for the former than for the latter. Such experiments have pointed out that the investigated samples involve a film with thickness of about 26 ± 4 nm (average of ten different values) composed by a fragile material, as it can be easily scratched by the tip, deposited on a harder substrate, that cannot be scratched by the tip in the same experimental conditions. The UV-vis spectrum was recorded on thin film electrodeposited onto ITO/PET substrate, using a Spectrophotometer Specord S 600 (Analytik Jena, Jena, Germany). The FT-IR spectrum was recorded on thin film electrodeposited onto ITO/glass substrate, using a FT-IR microscope (LUMOS, Bruker).

Pbis-Th2PC$_{60}$ sensor fabrication

Inkjet printing by a Dimatix™ DMP 2800 (Fujifilm Holdings America Corporation) and a commercial colloidal silver precursor (Novacentrix JS-A191) allow realizing silver electrodes for measuring the film resistance values. This instrument was equipped with user fillable piezo-driven inkjet print cartridges, each with 16 nozzles 254 µm spaced and 21.5 µm in diameter. The droplets were emitted at a jetting frequency of 2 kHz by using a previously optimized single-pulse waveform[44] (i.e. the voltage vs. time signal given as input to the piezoelectric actuator). The droplets center-to-center spacing was kept at 18 µm in order to favor an optimal droplets coalescence. To obtain the conductive silver pattern, the colloidal silver precursor was printed directly on the Pbis-Th2PC$_{60}$ thin film patterned on ITO/PET, preheated at 30°C and subsequently dried at 100 °C for one hour.

Resistance measurement

The piezoresistive property of the thin films was characterized by bending the sample on a motorized hinge (see **Figure 5c**). One part of the hinge is fastened with the holding construction, permitting to mount the sample in a stationary position. The second part is movable and connected directly to the shaft of the Qmot® QSH6018-65-28-210 precision micro-step motor (Trinamic Motion Control GmbH & Co. KG Hamburg, Germany). A custom-shaped guide screwed on the movable part of the hinge permitted to bend the sample, which slips in the guide without damaging the electrodeposited material in the bending angle interval comprised between 0° and 90°. The thicknesses of the ITO coating (about 130 nm) and the electrodeposited material (about 70-80 nm) are lower than the thickness of the PET substrate (about 120-130 µm). Thus, theoretical models analyzing the bending strain in plastic electronics devices[45] are applicable, approximating the strain exerted on the sample with $d_s/2R$ (where d_s is the PET substrate thickness and R is the radius of curvature). This equation, applied to the electrodeposited area when the sensor bent at 90°, permits to estimate a strain not exceeding 1.5%, considering also that the sample deformed at each angle without any stretching effect.[23] The quantitative estimation of bending induced strain is outside the scope of this work. A user interface developed with Labview® (National Instruments™, Austin, Texas, U.S.) was leveraged to synchronize the motor movements with a multimeter, model 34405A (Agilent Technologies, Inc), devoted to extracting the values of resistance for each bending angle.

Acknowledgements

References

[1] a) Z. He, C. Zhong, S. Su, M. Xu, H. Wu, Y. Cao, *Nat. Photonics.* **2012**, *6*, 591-595; b) K. G. Lim, S. Ahn, H. Kim, M. R. Choi, D. H. Huh, T. W. Lee, *Adv. Mater. Interfaces* **2016**, *3*, 1-7; c) J. H. Yim, S. Y. Joe, C. Pang, K. M. Lee, H. Jeong, J. Y. Park, Y. H. Ahn, J. C. De Mello, S. Lee, *ACS Nano* **2014**, *8*, 2857-2863; d) H. Hwan Jung, D. Ho Kim, C. Su Kim, T. S. Bae, K. Bum Chung, S. Yoon Ryu, *Appl. Phys. Lett.* **2013**, *102*, 17-22; e) C. Sartorio, V. Figà, P. Salice, D. Gragnato, S. Cataldo, M. Scopelliti, R. Improta, E. Menna, B. Pignataro, *Synth. Met.* **2017**, *229*, 7-15; f) P. Salice, C. Sartorio, A. Burlini, R. Improta, B. Pignataro, E. Menna, *J. Mater. Chem. C* **2015**, *3*, 303-312.

[2] a) J. Smith, W. Zhang, R. Sougrat, K. Zhao, R. Li, D. Cha, A. Amassian, M. Heeney, I. McCulloch, T. D. Anthopoulos, *Adv. Mater.* **2012**, *24*, 2441-2446; b) H. Chen, Y. Guo, G. Yu, Y. Zhao, J. Zhang, D. Gao, H. Liu, Y. Liu, *Adv. Mater.* **2012**, *24*, 4618-4622; c) Z. Yi, L. G. Bettini, G. Tomasello, P. Kumar, P. Piseri, I. Valitova, P. Milani, F. Soavi, F. Cicoira, *J. Polym. Sci., Part B: Polym. Phys.* **2017**, *55*, 96-103.

[3] a) C. Giordano, M. T. Todaro, M. Palumbo, L. Blasi, V. Errico, A. Salhi, A. Qualtieri, G. Gigli, A. Passaseo, M. De Vittorio, *Microelectron. Eng.* **2008**, *85*, 1170-1172; b) C. Steffens, A. N. Brezolin, J. Steffens, *Scanning* **2018**, *2018*, 4782685; c) N. Perinka, C. H. Kim, M. Kaplanova, Y. Bonnassieux, *Phys. Procedia* **2013**, *44*, 120-129.

[4] a) K. Nakabayashi, H. Mori, *Materials* **2014**, *7*, 3274-3290; b) T. Umeyama, H. Imahori, *Acc. Chem. Res.* **2019**, *52*, 2046-2055; c) A. Mohajeri, A. Omidvar, *PCCP* **2015**, *17*, 22367-22376; d) F. Giacalone, N. Martín, *Adv. Mater.* **2010**, *22*, 4220-4248; e) F. Giacalone, N. Martín, *Chem. Rev.* **2006**, *106*, 5136-5190; f) N. Martín, F. Giacalone, *Fullerene Polymers: Synthesis, Properties and Applications*, Wiley, **2009**.

[5] C. Sartorio, V. Campisciano, C. Chiappara, S. Cataldo, M. Scopelliti, M. Gruttadauria, F. Giacalone, B. Pignataro, *J. Mater. Chem. A* **2018**, *6*, 3884-3894.

[6] M. Lenes, S. W. Shelton, A. B. Sieval, D. F. Kronholm, J. C. Hummelen, P. W. M. Blom, *Adv. Funct. Mater.* **2009**, *19*, 3002-3007.

[7] a) E. Castro, O. Fernandez-Delgado, F. Arslan, G. Zavala, T. Yang, S. Seetharaman, F. D'Souza, L. Echegoyen, *New J. Chem.* **2018**, *42*, 14551-14558; b) K. M. Kaunisto, N. K. Subbaiyan, C. B. K.C, V. I. Chukharev, H. M. Hakola, T. K. Vuorinen, V. M. Manninen, N. V. Tkachenko, H. J. Lemmetyinen, F. D'Souza, *Synth. Met.* **2014**, *195*, 193-200.

[8] F. Steiner, S. Foster, A. Losquin, J. Labram, T. D. Anthopoulos, J. M. Frost, J. Nelson, *Mater. Horizons* **2015**, *2*, 113-119.

[9] N. M. Sangeetha, N. Decorde, B. Viallet, G. Viau, L. Ressier, *J. Phys. Chem. C* **2013**, *117*, 1935-1940.

[10] a) Y. Kanda, *Sensors Actuators, A Phys.* **1991**, *28*, 83-91; b) G. Saggio, E. Verona, P. Di Rosa, S. La Monica, R. Salotti, L. Schirone, *Mater. Sci. Eng., B* **1995**, *29*, 176-180.

[11] X. Liu, G. Su, Q. Guo, C. Lu, T. Zhou, C. Zhou, X. Zhang, *Adv. Funct. Mater.* **2018**, *28*, 1706658.

[12] a) G. Arrabito, V. Errico, Z. Zhang, W. Han, C. Falconi, *Nano Energy* **2018**, *46*, 54-62; b) V. Errico, G. Arrabito, S. R. Plant, P. G. Medaglia, R. E. Palmer, C. Falconi, *Sci. Rep.* **2015**, *5*, 12336; c) Z. L. Wang, J. Song, *Science* **2006**, *312*, 242-246; d) C. L. Hsu, K. C. Chen, *J. Phys. Chem. C* **2012**, *116*, 9351-9355.

[13] a) X. Shi, S. Liu, Y. Sun, J. Liang, Y. Chen, *Adv. Funct. Mater.* **2018**, *28*, 1-10; b) G. Georgousis, E. Kontou, A. Kyritsis, P. Pissis, M. Mičušík, M. Omastová, *J. Reinf. Plast. Compos.* **2018**, *37*, 1085-1098.

[14] a) A. Leoni, V. Stornelli, G. Ferri, V. Errico, M. Ricci, A. Pallotti, G. Saggio, *PRIME 2018 - 14th Conference on Ph.D. Research in Microelectronics and Electronics* **2018**, 8430362; b) V. Stornelli, A. Leoni, G. Ferri, V. Errico, M. Ricci, A. Pallotti, G. Saggio, *2018 3rd International Conference on Smart and Sustainable Technologies, SpliTech 2018* **2018**, 8448343.

[15] P. Nie, R. Wang, X. Xu, Y. Cheng, X. Wang, L. Shi, J. Sun, *ACS Appl. Mater. Interfaces* **2017**, *9*, 14911-14919.

[16] a) W. Chen, Y. Bu, D. Li, Y. Liu, G. Chen, X. Wan, N. Li, *J. Mater. Chem. C* **2020**, *8*, 900-908; b) G. Saggio, A. Lazzaro, L. Sbernini, F. M. Carrano, D. Passi, A. Corona, V. Panetta, A. L. Gaspari, N. Di Lorenzo, *J. Surg. Educ.* **2015**, *72*, 910-917.

[17] G. Saggio, M. Bizzarri, *Aerosp. Sci. Technol.* **2014**, *39*, 666-674.

[18] a) L. Pan, A. Chortos, G. Yu, Y. Wang, S. Isaacson, R. Allen, Y. Shi, R. Dauskardt, Z. Bao, *Nat. Commun.* **2014**, *5*, 1-8; b) V. Errico, G. Arrabito, E. Fornetti, C. Fuoco, S. Testa, G. Saggio, S. Rufini, S. Cannata, A. Desideri, C. Falconi, C. Gargioli, *ACS Appl. Mater. Interfaces* **2018**, *10*, 14097–14107.

[19] G. Saggio, G. Orengo, *Sensors Actuators, A Phys.* **2018**, *273*, 221-231.

[20] H.-R. Lim, H. S. Kim, R. Qazi, Y.-T. Kwon, J.-W. Jeong, W.-H. Yeo, *Adv. Mater.* **2020**, *32*, 1901924.

[21] a) G. Saggio, F. Riillo, L. Sbernini, L. R. Quitadamo, *Smart Mater. Struct.* **2015**, *25*, 013001; b) A. Rashid, O. Hasan, *Microelectron. J.* **2019**, *88*, 173-183.

[22] a) G. Saggio, G. Orengo, A. Pallotti, V. Errico, M. Ricci, *2018 Int. Symp. Networks, Comput. Commun. (ISNCC 2018)* **2018**, 8531054; b) G. Saggio, G. Orengo, A. Pallotti, V. Errico, M. Ricci, *MeMeA 2018 - 2018 IEEE International Symposium on Medical Measurements and Applications, Proceedings* **2018**, 8438767; c) M. Ricci, M. Terribili, F. Giannini, V. Errico, A. Pallotti, C. Galasso, L. Tomasello, S. Sias, G. Saggio, *J. Biomech.* **2019**, *83*, 243-252; d) G. Saggio, L. Sbernini, *MeMeA 2011 - 2011 IEEE International Symposium on Medical Measurements and Applications, Proceedings* **2011**, 13-17.

[23] G. Latessa, F. Brunetti, A. Reale, G. Saggio, A. Di Carlo, *Sensors Actuators, B Chem.* **2009**, *139*, 304-309.

[24] G. Ge, Y. Zhang, J. Shao, W. Wang, W. Si, W. Huang, X. Dong, *Adv. Funct. Mater.* **2018**, *28*, 1-8.

[25] Z. Yang, Y. Pang, X. L. Han, Y. Yang, Y. Yang, J. Ling, M. Jian, Y. Zhang, T. L. Ren, *ACS Nano* **2018**, *12*, 9134-9141.

[26] S. Lu, J. Ma, K. Ma, X. Wang, S. Wang, X. Yang, H. Tang, *Appl. Phys. A Mater. Sci. Process.* **2019**, *125*, 1-11.

[27] a) T. Lee, Y. W. Choi, G. Lee, P. V. Pikhitsa, D. Kang, S. M. Kim, M. Choi, *J. Mater. Chem. C* **2016**, *4*, 9947-9953; b) S. H. Hwang,

H. J. Ahn, J. C. Yoon, J. H. Jang, Y. B. Park, *J. Mater. Chem. C* **2013**, *1*, 7208-7214.

[28] a) D. J. Lipomi, M. Vosgueritchian, B. C. K. Tee, S. L. Hellstrom, J. A. Lee, C. H. Fox, Z. Bao, *Nat. Nanotechnol.* **2011**, *6*, 788-792; b) Z. Liu, D. Qi, P. Guo, Y. Liu, B. Zhu, H. Yang, Y. Liu, B. Li, C. Zhang, J. Yu, B. Liedberg, X. Chen, *Adv. Mater.* **2015**, *27*, 6230-6237; c) S. H. Bae, Y. Lee, B. K. Sharma, H. J. Lee, J. H. Kim, J. H. Ahn, *Carbon* **2013**, *51*, 236-242.

[29] a) P. Piotrowski, K. Zarębska, M. Skompska, A. Kaim, *Electrochim. Acta* **2014**, *148*, 145-152; b) V. Figà, C. Chiappara, F. Ferrante, M. P. Casaletto, F. Principato, S. Cataldo, Z. Chen, H. Usta, A. Facchetti, B. Pignataro, *J. Mater. Chem. C* **2015**, *3*, 5985-5994; c) J. Heinze, B. A. Frontana-Uribe, S. Ludwigs, *Chem. Rev.* **2010**, *110*, 4724-4771.

[30] M. Maggini, G. Scorrano, M. Prato, *J. Am. Chem. Soc.* **1993**, *115*, 9798-9799.

[31] a) K. Kordatos, S. Bosi, T. Da Ros, A. Zambon, V. Lucchini, M. Prato, *J. Org. Chem.* **2001**, *66*, 2802-2808; b) A. Hirsch, I. Lamparth, H. R. Karfunkel, *Angew. Chemie Int. Ed. English* **1994**, *33*, 437-438; c) F. Diederich, R. Kessinger, *Acc. Chem. Res.* **1999**, *32*, 537-545; d) A. Hirsch, *Chem. Rec.* **2005**, *5*, 196-208.

[32] Q. Lu, D. I. Schuster, S. R. Wilson, *J. Org. Chem.* **1996**, *61*, 4764-4768.

[33] R. J. Waltman, J. Bargon, A. F. Diaz, *J. Phys. Chem.* **1983**, *87*, 1459-1463.

[34] N. Elgrishi, K. J. Rountree, B. D. McCarthy, E. S. Rountree, T. T. Eisenhart, J. L. Dempsey, *J. Chem. Educ.* **2018**, *95*, 197-206.

[35] M. Fathy, S. Elyamny, S. Mahmoud, A. E. H. B. Kashyout, *Int. J. Electrochem. Sci.* **2015**, *10*, 6030-6043.

[36] K. Bieńkowski, M. Strawski, M. Szklarczyk, *J. Electroanal. Chem.* **2011**, *662*, 196-203.

[37] J. A. Del-Oso, B. A. Frontana-Uribe, J.-L. Maldonado, M. Rivera, M. Tapia-Tapia, G. Roa-Morales, *J. Solid State Electrochem.* **2018**, *22*, 2025-2037.

[38] S. A. Spanninga, D. C. Martin, Z. Chen, *J. Phys. Chem. C* **2009**, *113*, 5585-5592.

[39] A. Cravino, N. S. Sariciftci, M. Barcu, B. Cuadra, A. K. Rai, P. Cheng, L. T. Scott, N. S. Sariciftci, C. J. Brabec, N. S. Sariciftci, *J. Mater. Chem.* **2002**, *12*, 1931-1943.

[40] X.-w. Zhang, Y. Pan, Q. Zheng, X.-s. Yi, *J. Polym. Sci., Part B: Polym. Phys.* **2000**, *38*, 2739-2749.

[41] a) Y. Cheng, R. Wang, J. Sun, L. Gao, *Adv. Mater.* **2015**, *27*, 7365-7371; b) S. Lu, S. Wang, G. Wang, J. Ma, X. Wang, H. Tang, X. Yang, *Sensors Actuators, A Phys.* **2019**, *295*, 200-209.

[42] U. Lang, N. Naujoks, J. Dual, *Synth. Met.* **2009**, *159*, 473-479.

[43] All attempts to electropolymerize this mixture failed.

[44] a) G. Arrabito, F. Cavaleri, V. Montalbano, V. Vetri, M. Leone, B. Pignataro, *Lab on a Chip* **2016**, *16*, 4666-4676; b) C. Miccichè, G. Arrabito, F. Amato, G. Buscarino, S. Agnello, B. Pignataro, *Anal. Methods* **2018**, *10*, 3215-3223.

[45] T. Sekitani, Y. Kato, S. Iba, H. Shinaoka, T. Someya, T. Sakurai, S. Takagi, *Appl. Phys. Lett.* **2005**, *86*, 1-3.

Entry for the Table of Contents

Low bending
High response
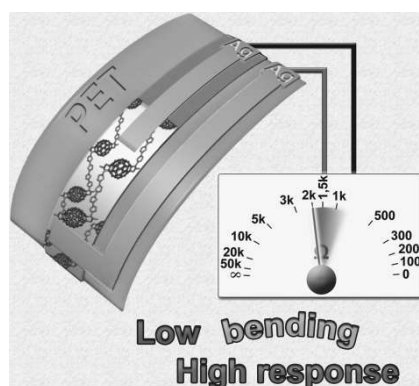
A new semitransparent bithiophene-fulleropyrrolidine thin film was electropolymerized by chronoamperometry on flexible ITO/PET substrates. The polymeric system was characterized by FT-IR, XPS, CV and optical techniques, showing transmittance of about 78% and excellent responsivity as bending sensor at low angles (10°-30°). At larger bending angles (40°-90°), the response was lower in accordance with piezoresistive sensing based on grains separation. This novel material opens up applications for bending sensor requiring high precision for small bending angles.